Supporting Information

An Indium-Induced-Synthesis $In_{0.17}Ru_{0.83}O_2$ Nanoribbon as Highly Active Electrocatalysts for Oxygen Evolution in Acidic Media at High Current Densities above 400 mA cm^{-2}

Shi Chen[1†], Changlai Wang [1†], Feiyue Gao [1], Yang Yang[1], Minxue Huang[1], Huigang Tong[1], Zhiyu Cheng[1], Pengcheng Wang[1], Peichen Wang[1], Jinwei Tu[1], Xuehao Zeng[1] and Qianwang Chen[1,2*]

[1]Hefei National Laboratory for Physical Science at Microscale and Department of Materials Science & Engineering, University of Science and Technology of China, Hefei 230026, China

[2] Anhui Province Key Laboratory of Condensed Matter Physics at Extreme Conditions, High Magnetic Field Laboratory of Chinese, Academy of Sciences, Hefei 230031, China

† These authors contributed equally to this work.

[*]Correspondence to: cqw@ustc.edu.cn.

Keywords: RuO_2 nanoribbon, electrocatalysts, oxygen evolution reaction, DFT calculation.

Contents

Number of pages: 20

Number of figures: 26

Number of tables: 7

Figures:

7. Reference

1. Experimental section

Materials: All reagents are of analytical grade and used without purification. Indium(III) chloride tetrahydrate ($InCl_3$•$4H_2O$), Ruthenium chloride hydrate ($RuCl_3$•xH_2O), ethanol absolute (C_2H_5OH) was purchased from Sinopharm Chemical Reagent limited corporation. Benzene-1,3,5-Benzenetricarboxylic acid ($C_9H_6O_6$, BTC) were purchased from J&K Scientific Ltd. The deionized water used throughout all experiments was purified through a Millipore system.

InRu-BTC, *Ru-BTC* and *In-BTC* synthesis: The typical synthetic experiment of *InRu-BTC* was as follows: Solution A: 439.86 mg $InCl_3 \cdot 4H_2O$ and 103.72 mg $RuCl_3$•xH_2O were dissolved in deionized water (25 mL). Solution B: 420.28 mg BTC was dissolved in ethanol (15 ml). Then, the solution B was added to the solution A slowly and regularly with a syringe under agitated stirring. The mixture was stirred for 30 min and was transferred into a 50 mL Teflon-lined steel reactor, then the reactor was heated to 160 °C for 12 h. The resulting black sample was collected by centrifugation, washed three times with deionized water and one time with ethanol, and thus dried in a vacuum oven at 60 °C for 12 h. The synthetic experiments of *Ru-BTC* and *In-BTC* are exactly the same as the above method except that $InCl_3 \cdot 4H_2O$ or $RuCl_3$•xH_2O is not added in Solution A.

$In_xRu_yO_2$-*n* and RuO_2-*350* synthesis: The preparation of the OER electrocatalysts were carried out as following: 50 mg of InRu-BTC were heated at different temperature (250 °C, 350 °C, 450 °C) for 4 h in the air atmosphere and the heating rate is 5 °C/min, values of x, y are determined by results of Inductively Coupled Plasma Mass Spectrometry (ICP-MS) as well, so the products are named $In_{0.14}Ru_{0.86}O_2$-*250*, $In_{0.17}Ru_{0.83}O_2$-*350*, $In_{0.18}Ru_{0.82}O_2$-*450*, respectively. Besides, Ru-BTC was heated at 350 °C for 4 h in the air atmosphere and the heating rate is 5 °C/min, named RuO_2-*350*.

In_2O_3 synthesis: 50 mg of In-BTC were heated at 500 °C for 4 h in the air atmosphere and the heating rate is 5 °C/min, named In_2O_3.

2. Materials characterization

The powder X-ray diffraction (XRD) patterns of the samples were collected from a Panalytical, X`Pert PRO MPD X-ray diffractometer equipped with Cu Kα radiation (λ=1.54178Å). Transmission electron microscopy (TEM) images were recorded with a Hitachi H-7650 transmission electron microscope using an accelerating voltage of 200 kV, and a high resolution transmission electron microscope (HRTEM) (JEOL-2011) was operated at an acceleration voltage of 200 kV. X-ray photoelectron spectroscopy (XPS) was conducted on an ESCALAB 250 X-ray photoelectron spectrometer instrument. The specific surface area was evaluated at 77 K using the Brunauer-Emmett-Teller (BET) method (Micromeritic TriStar II 3020 V1.03 instrument), while the pore volume and pore size were calculated according to the Barrett-Joyner-Halenda

(BJH) formula applied to the adsorption branch. Inductively coupled plasma-atomic emission spectrometer (ICP-AES) were conducted to determine the Ru and In concentrations of the samples with an Optima 7300 DV instrument. Ultraviolet photoemission spectroscopy (UPS) measurements were performed at the Catalysis and Surface Science Endstation of the National Synchrotron Radiation Laboratory (NSRL) in Hefei, China. A sample bias of −10 V was applied to observe the secondary electron cutoff. The gas produced during the reaction is continuously fed into the gas chromatography (Agilent 7890B) for the analysis of its composition.

3. Electrocatalytic measurements details

All electrochemical experiments were performed in a standard three-electrode cell at room temperature. The cell consists of a glassy carbon working electrode (GC electrode, 3 mm in diameter，loading ~0.275 mg cm^{-2}), an Ag/AgCl reference electrode, and a graphite rod counter electrode. All potentials in this study are given relative to the reversible hydrogen electrode (RHE) after transformation (E_{RHE} = $E_{Ag/AgCl}$ + 0.197+0.0591pH). Overpotential η (V) = E (RHE) -1.23 V. The working electrodes were prepared by applying catalyst ink onto glassy carbon (GC). The GC eleatrodes should be carefully polished with Al_2O_3 powders with a size of 0.05 μm and rinsed with deionized water before adding catalysts onto the GC. Typically, 4 mg of catalyst was dispersed in a solution containing 1 ml of the ethanol solvent and 30μL Nafion solution (Sigma Aldrich, 5 wt%) and ultrasonicated for at least 30 minutes to form a uniform catalyst ink. A total of 5 μL of well-dispersed catalyst ink was applied onto the pre-polished GC disk. The prepared electrodes were dried at room temperature before electrochemical tests. The polarization curves were collected of working electrodes were collected in O_2 saturated 0.5 M H_2SO_4 a with a scan rate of 5 mV /s, after the signals were stabilized via. several scans. Cyclic voltammetry (CV) was conducted in acidic media in the potential region from 0.9 to 1.4 V versus Ag/AgCl electrode at a sweep rate of 100 mV /s for 5000 to investigate the long-term cycling stability. All the electrolyses were conducted at room temperature. Besides, chronopotentiometric electrolysis of the working electrode was held at a current density of 10 mA cm^{-2} for 20 hours. All the electrolysis was conducted at room temperature, and IR correction was not applied in all measurements.Nyquist plots of electrochemical impedance spectroscopy (EIS) measurements were collected in frequency range of 0.01-10^6 Hz at corresponding open circuit voltages vs. Ag/AgCl electrode. The electrical double layer capacitor (C_{dl}) were measured from double-layer charging curves using cyclic voltammograms in a small potential range of 0.853-0.953 V vs. Ag/AgCl electrode with scan rate from 10 to 100 mV/s.[1] The plot of the corresponding current density (△j/2 at 0.903 V vs. Ag/AgCl electrode) against scan rate has a linear relationship and its slope is the C_{dl}. The ECSA is calculated from the double layer capacitance according to:[2]

$$ECSA = C_{dl} \cdot S/Cs \quad (1)$$

Where Cs is the specific capacitance of the sample. We use general specific capacitances of Cs = 0.035 mF cm^{-2} based on typical reported values, S is the geometric area of the electrode.[2]The roughness factor (RF) is calculated by dividing ECSA by 0.071 cm^2, the geometric area of the electrode.

The values of turnover frequency (TOF) are calculated using the following formula, assuming that all Ru ions in the catalysts are active and contribute to the catalytic reaction (the lowest TOF values were calculated).[3]

$$TOF = JS/ (4Fn) \quad (2)$$

Where J is the measured current density at an overpotential of 300 mV; S (0.071 cm^2) is the surface area of GCE; the number of 4 means 4 electrons transfer in OER; F is Faraday constant (96485 C mol^{-1}), and n is the molar number of Ru ions calculated from mass loading (0.275 mg cm^{-2}) and ICP results of catalyst.

The significance of TON is the ratio of the number of moles of reactant transformation to the number of moles of catalyst, and the relation between TON and TOF is TOF value multiplied by corresponding reaction time.

4. Finite-element method simulations.

In our work, the electrical double layer was modelled using the Gouy–Chapman–Stern model. The diffusion layer consists of cations and anions, which was established as the result of a dynamic equilibrium between electrostatic forces and diffusion. The Poisson–Nerst–Planck equations were solved in the steady state.[4] Two-dimensional nanoribbon and sphere were built to represent the XXX and YYY in this work. Conventional triangular meshes is used for all simulations, and the meshes are set to the densest grid of electrode surfaces.

5. Calculation details

All the calculations were based on density functional theory by using the Vienna ab-initio simulation package (VASP).[5] The generalized gradient approximation (GGA) with the function of Perdew-Becke-Ernzerhof (PBE) was employed to describe the electron interaction energy of exchange correlation.[6] The projector augmented wave was applied to describe the electron-ion interaction and the plane-wave energy cutoff was set to 400 eV. The convergences of energy and force were set to 1×10^{-5} eV and 0.01eV/Å, respectively. Brillouin zone sampling was employed using a Monkhorst-Packing grid with 3 × 3 × 1. The free energy diagrams of the oxygen evolution reaction (OER) have been calculated according to the method developed by Rossmeisl et al.[7] The free energies of the intermediates are calculated as follows:

$\Delta G = \Delta E + \Delta ZPE - T\Delta S + eU$

where ΔE is the binding energy of adsorption species *OOH, *O and *OH, ΔZPE is the change in zero-point energy, T is the temperature (298.15 K), and ΔS is the change in entropy, U is applied potentials. Zero-point energy and entropies of the adsorbed species were calculated from the vibrational frequencies.

6. Supplementary Figures and Tables

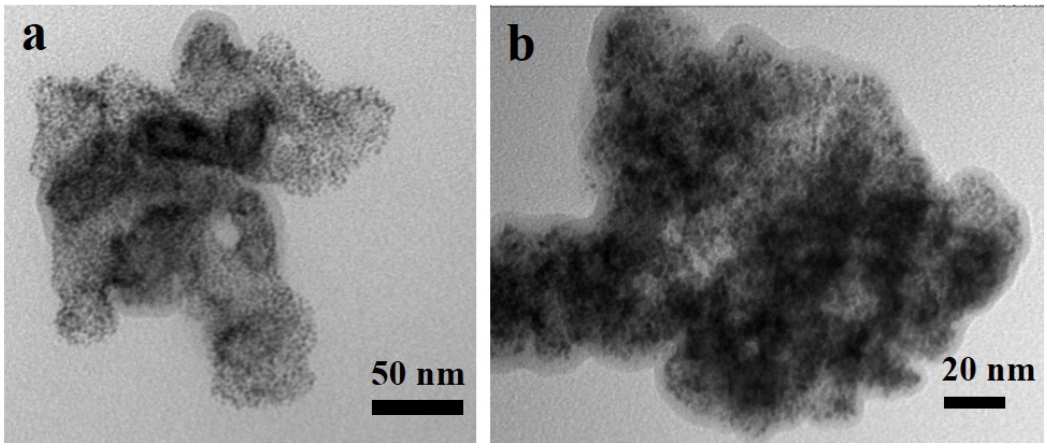

Figure S1. TEM images of the as-prepared InRu-BTC.

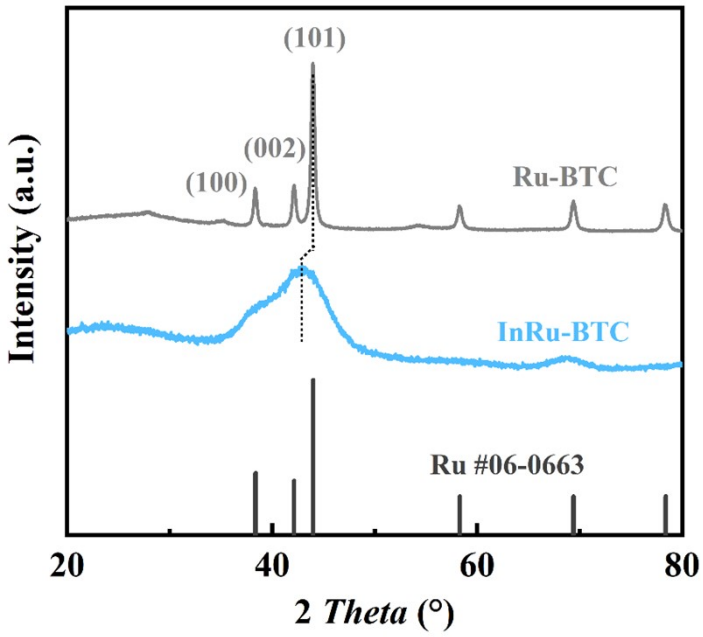

Figure S2. The XRD patterns of as-prepared Ru-BTC and InRu-BTC samples.

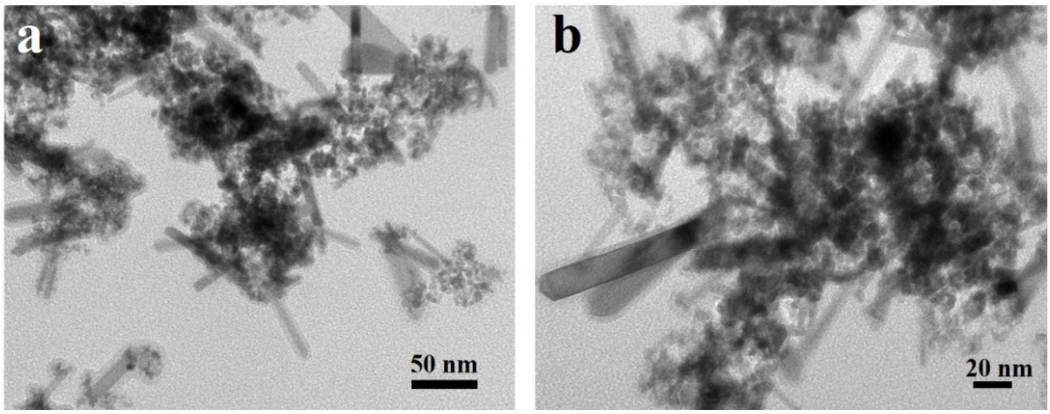

Figure S3. TEM images of the as-prepared $In_{0.14}Ru_{0.86}O_2$-250.

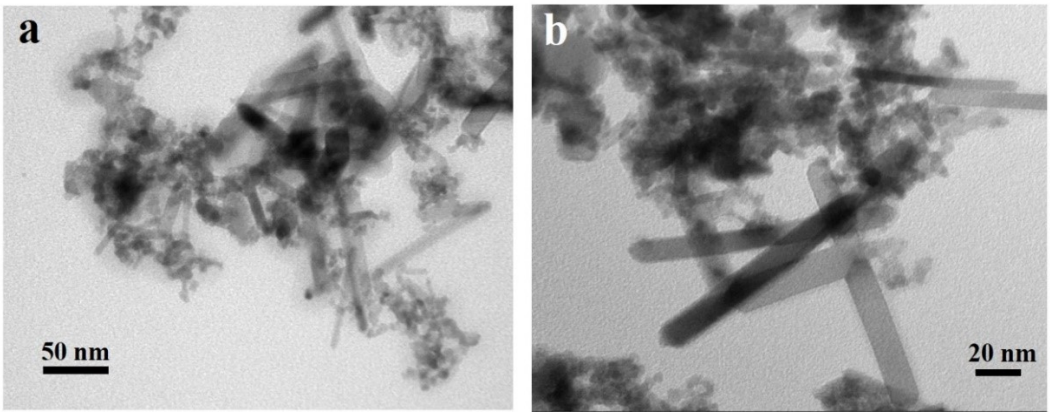

Figure S4. TEM images of the as-prepared $In_{0.17}Ru_{0.83}O_2$-350.

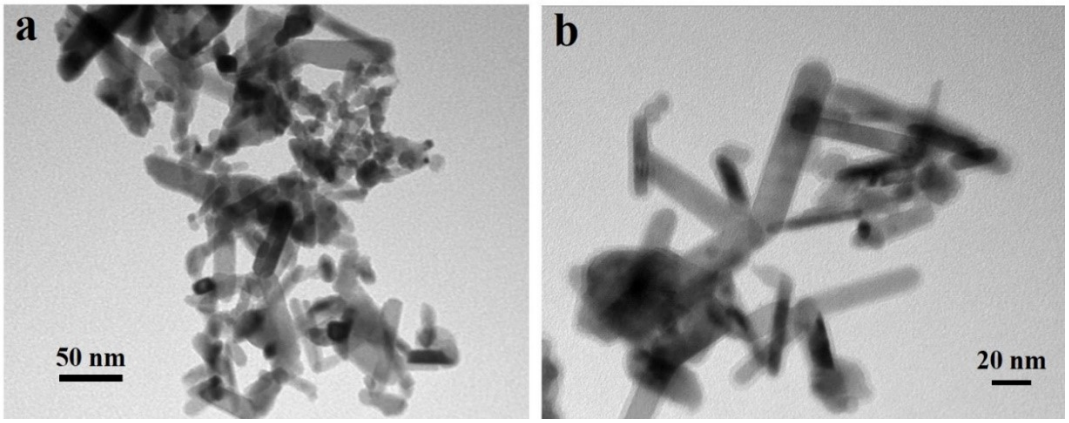

Figure S5. TEM images of the as-prepared $In_{0.18}Ru_{0.82}O_2$-450.

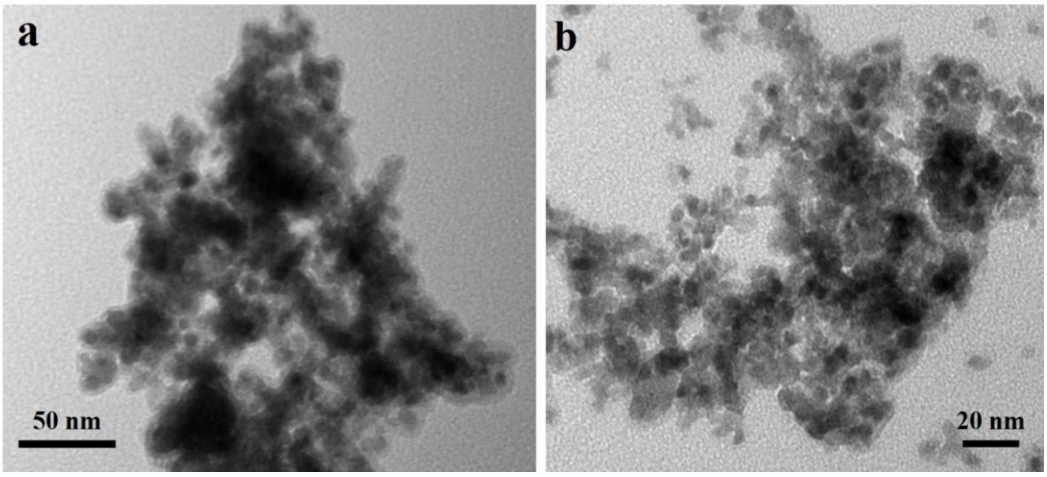

Figure S6. TEM images of the as-prepared RuO_2-350.

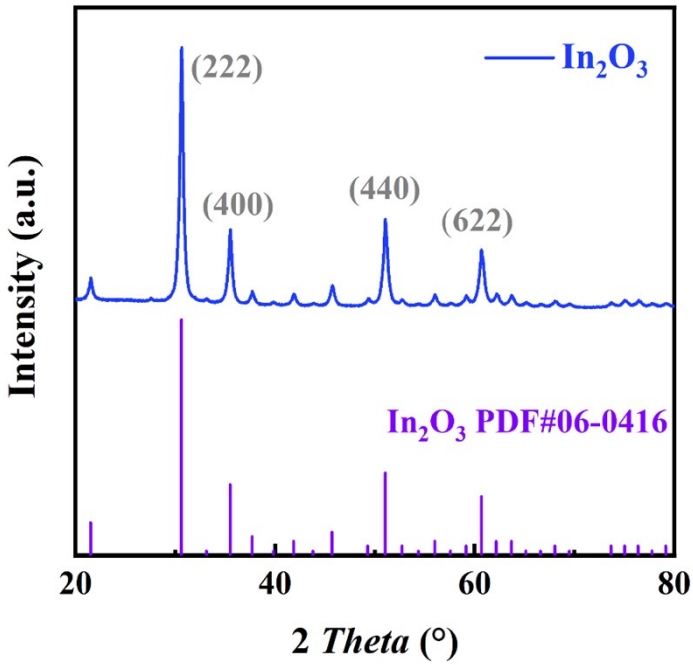

Figure S7. The XRD patterns of as-prepared In_2O_3 sample.

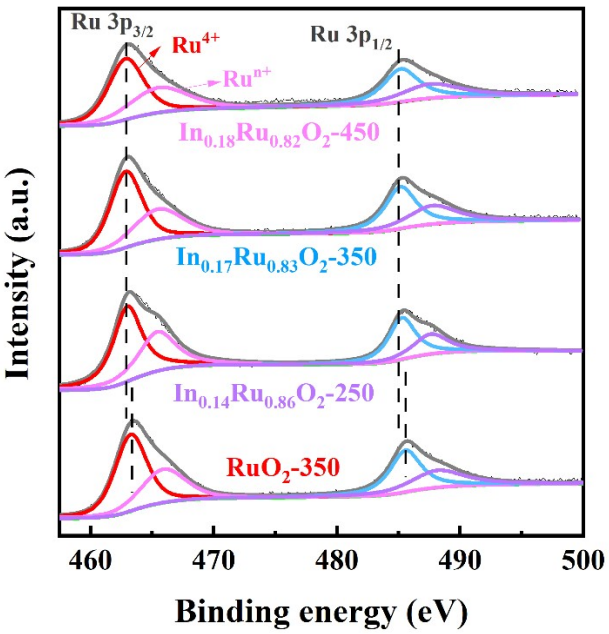

Figure S8. High-resolution spectra of XPS of RuO_2-350 and $In_xRu_yO_2$-n samples for Ru 3p.

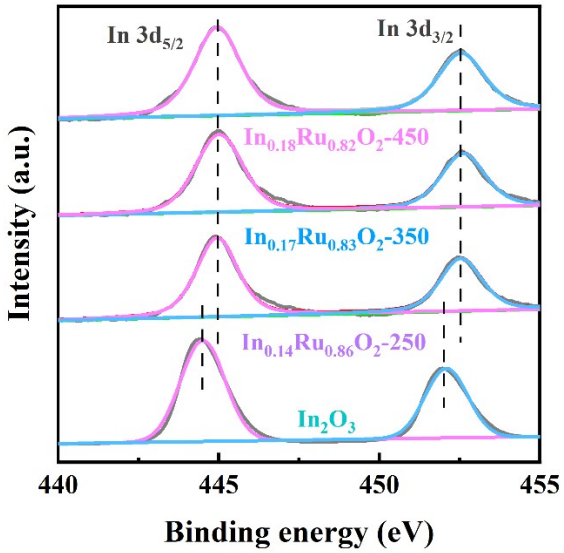

Figure S9. High-resolution spectra of XPS of In_2O_3 and $In_xRu_yO_2$-n samples for In 3d.

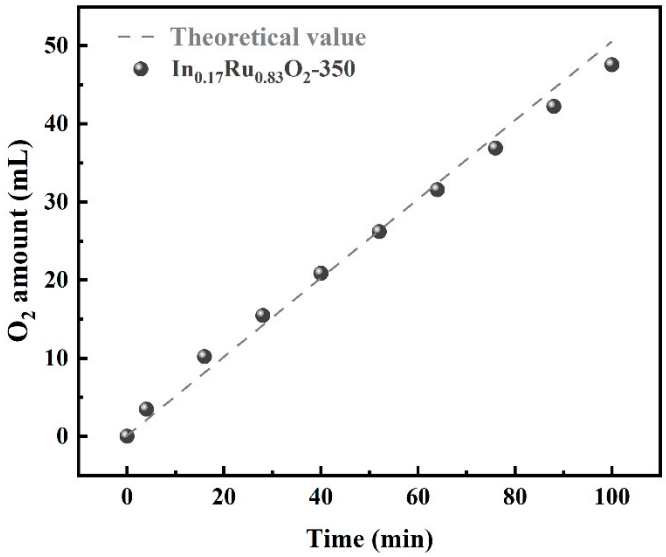

Figure S10. GC-measured O_2 amounts at different time intervals.

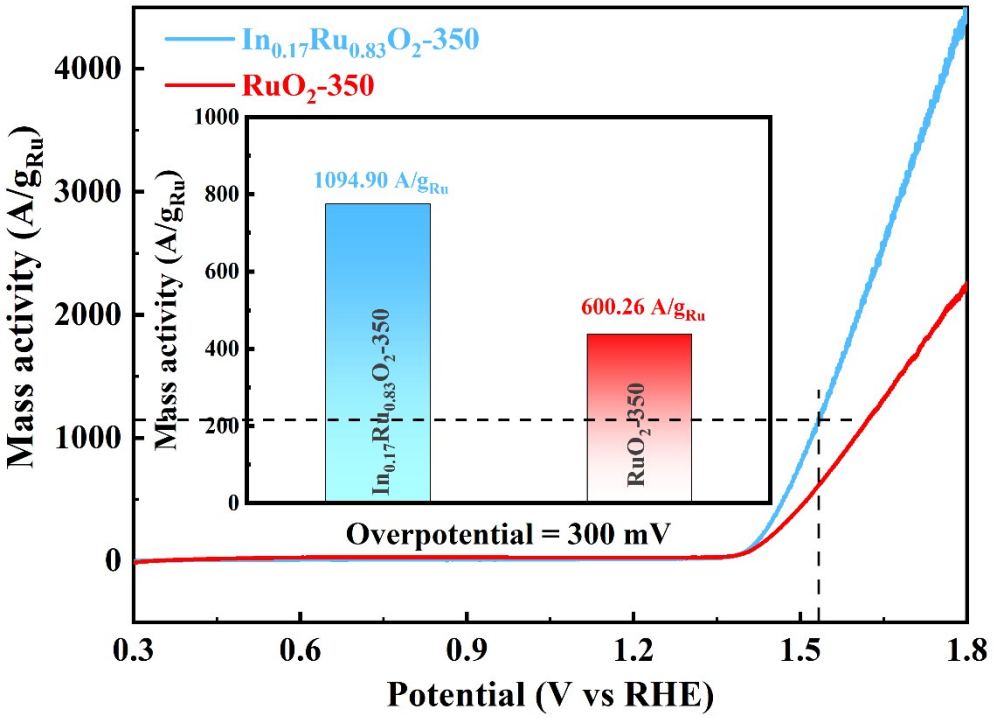

Figure S11. OER mass activities of overpotential of 300 mV by normalized by the Ru metal mass.

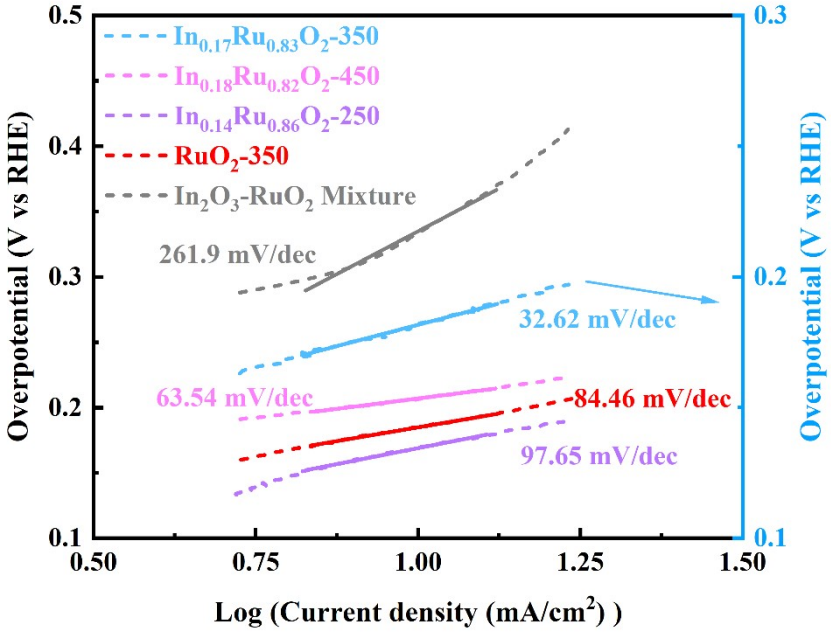

Figure S12. Tafel plots of RuO_2-350 and $In_xRu_yO_2$-n samples.

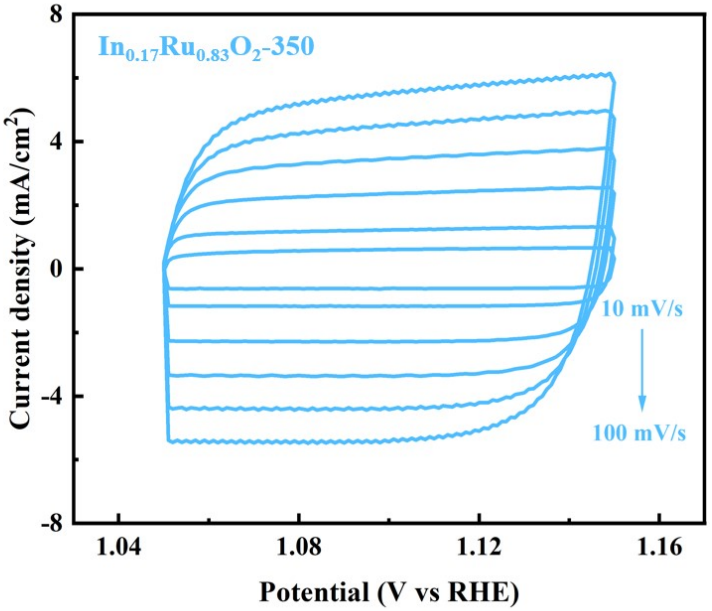

Figure S13. CV curves measured within the range of 1.05 to 1.15 V *vs.* RHE with scan rate from 10 to 100 mV s^{-1} of $In_{0.17}Ru_{0.83}O_2$-350.

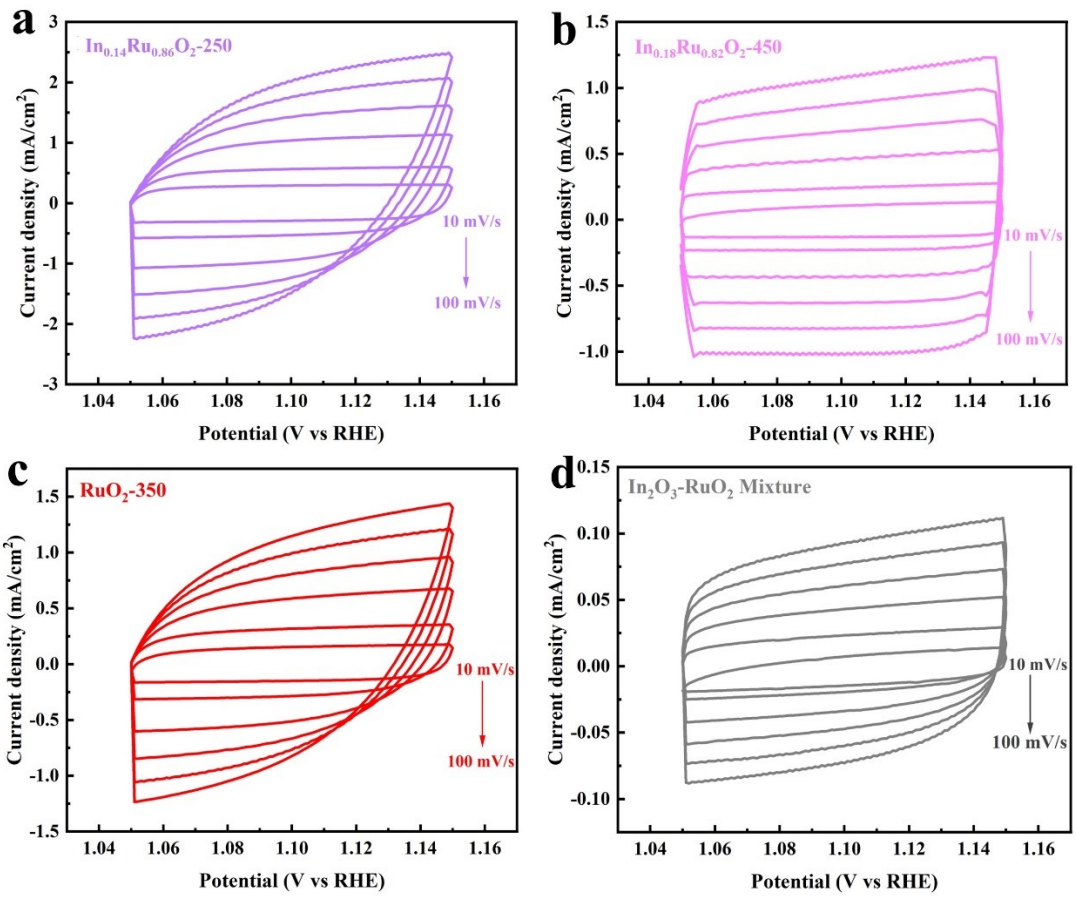

Figure S14. CV curves measured within the range of 1.05 to 1.15 V *vs.* RHE with scan rate from 10 to 100 mV s^{-1} of (a) $In_{0.14}Ru_{0.86}O_2$-250, (b) $In_{0.18}Ru_{0.82}O_2$-450, (c) RuO_2-350 and (d) In_2O_3-RuO_2 Mixture.

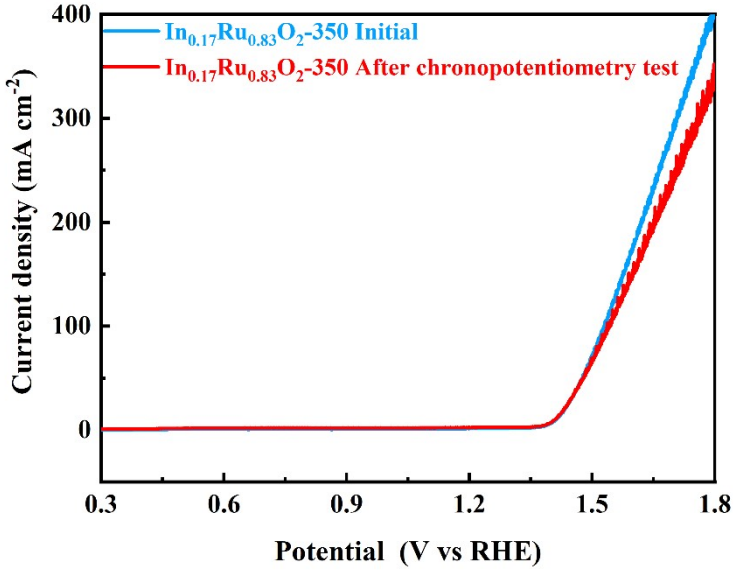

Figure S15. OER polarization curves of $In_{0.17}Ru_{0.83}O_2$-350 before and after chronopotentiometry test.

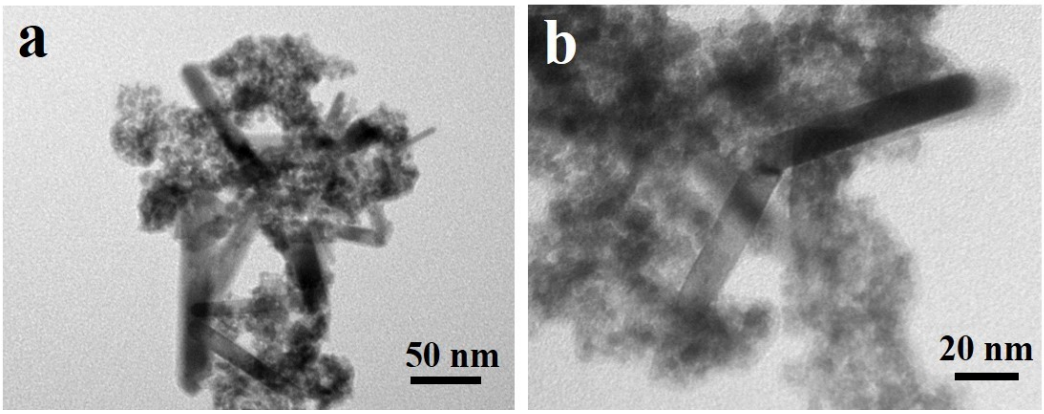

Figure S16. TEM images of the $In_{0.17}Ru_{0.83}O_2$-350 after OER stability test.

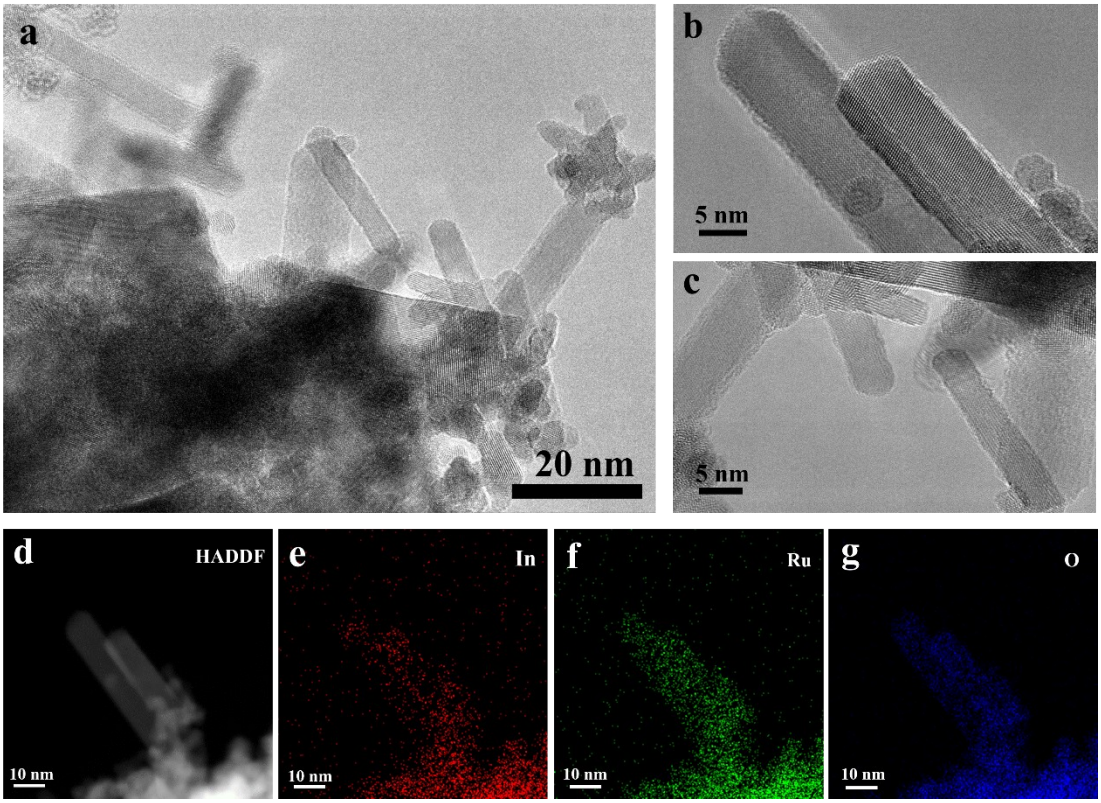

Figure S17. HRTEM images of the $In_{0.17}Ru_{0.83}O_2$-350 after OER stability test.

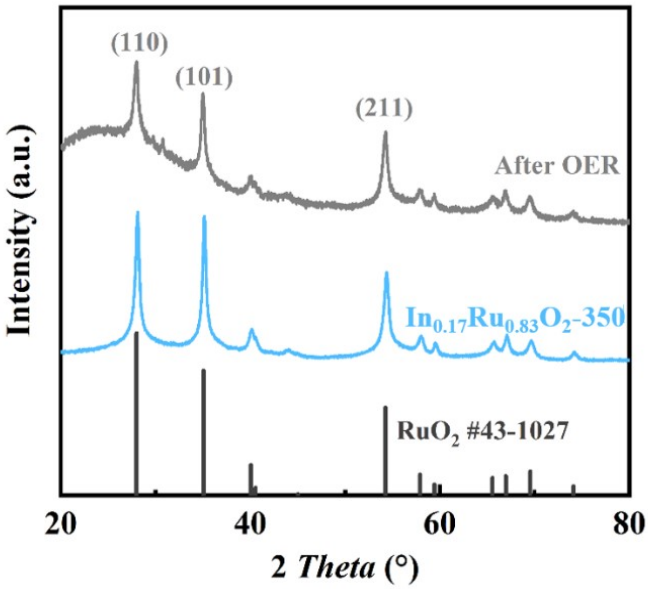

Figure S18. The XRD patterns of $In_{0.17}Ru_{0.83}O_2$-350 sample before and after OER stability test.

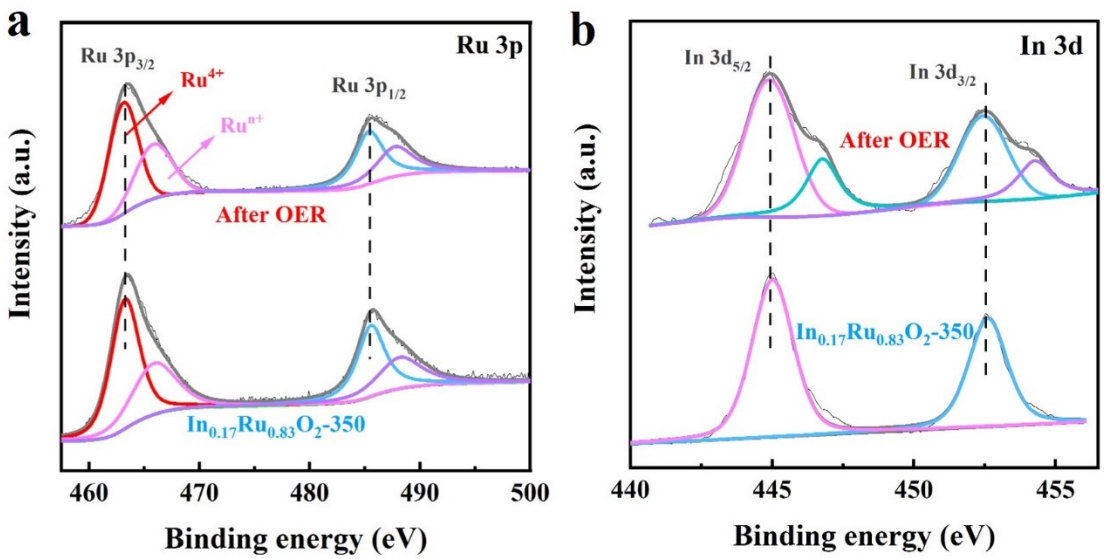

Figure S19. High-resolution spectra of XPS of $In_{0.17}Ru_{0.83}O_2$-350 samples before and after OER stability test for (a) Ru 3p and (b) In 3d.

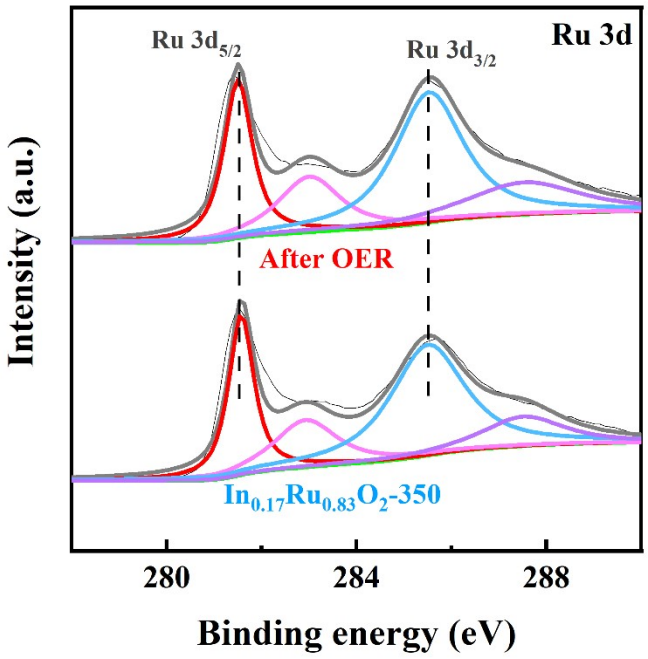

Figure S20. High-resolution spectra of XPS of $In_{0.17}Ru_{0.83}O_2$-350 samples before and after OER for Ru 3d.

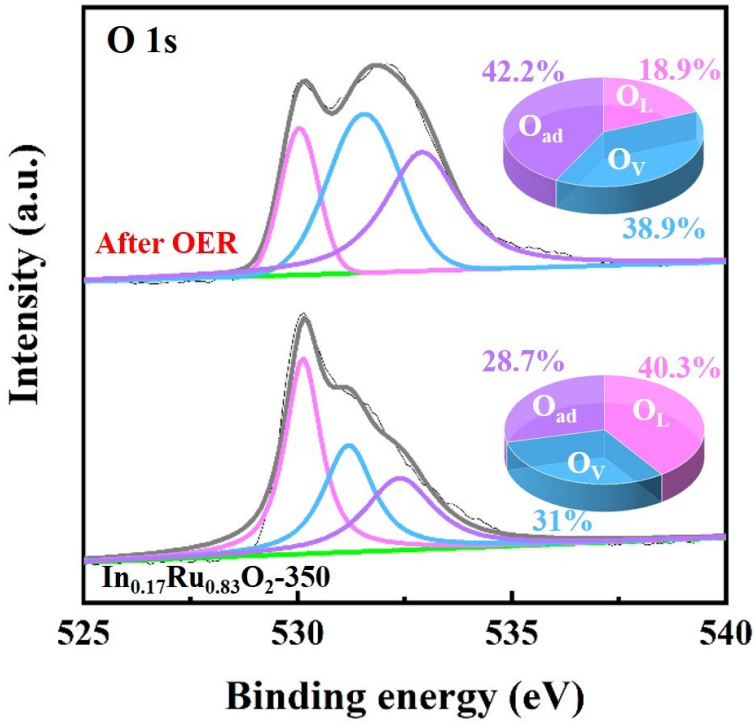

Figure S21. High-resolution spectra of XPS of $In_{0.17}Ru_{0.83}O_2$-350 samples before and after OER stability test for O 1s.

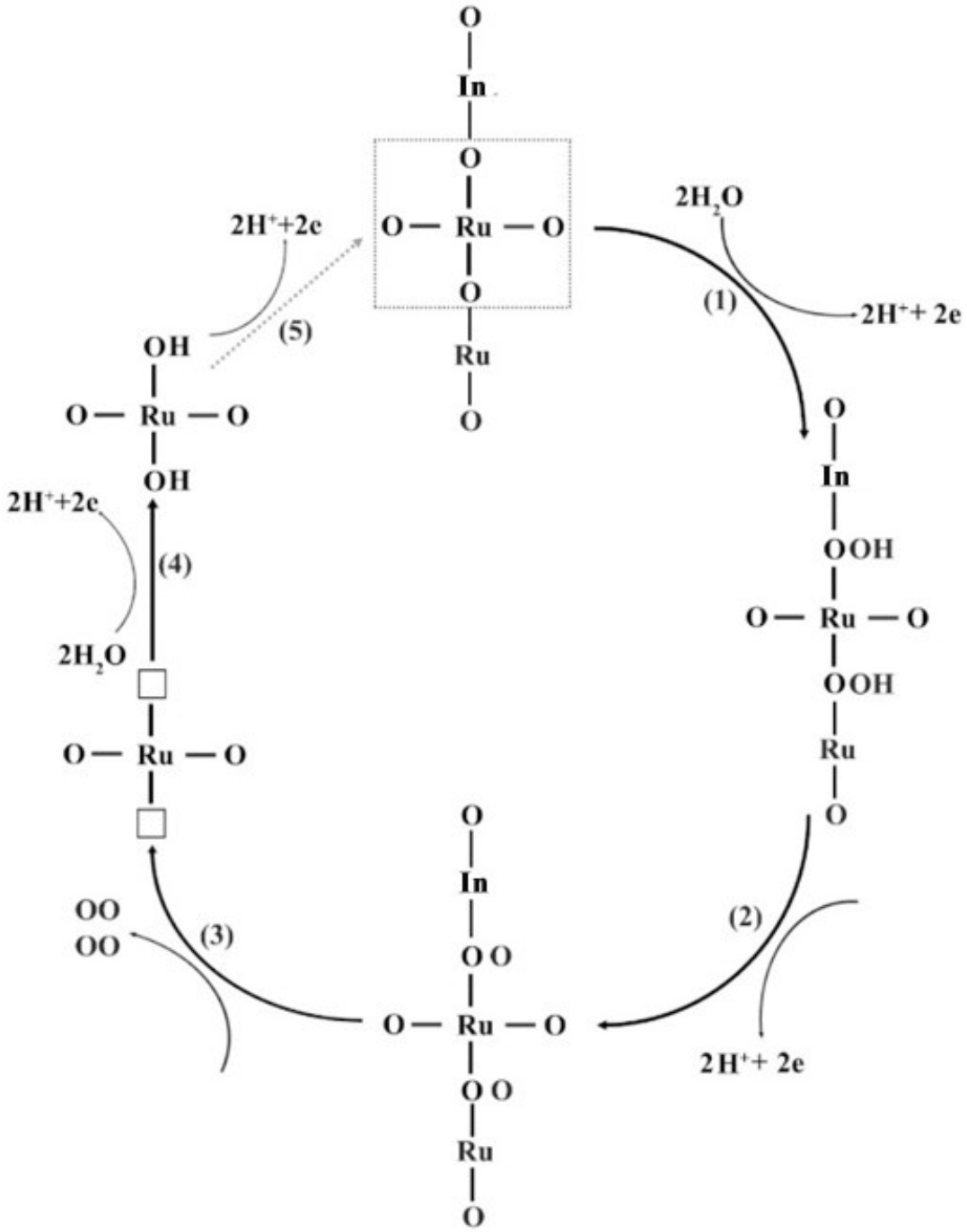

Figure S22. The speculated mechanism of Ru atom on the $InRuO_2$ surface due to Lattice Oxygen Evolution Reaction (LOER).

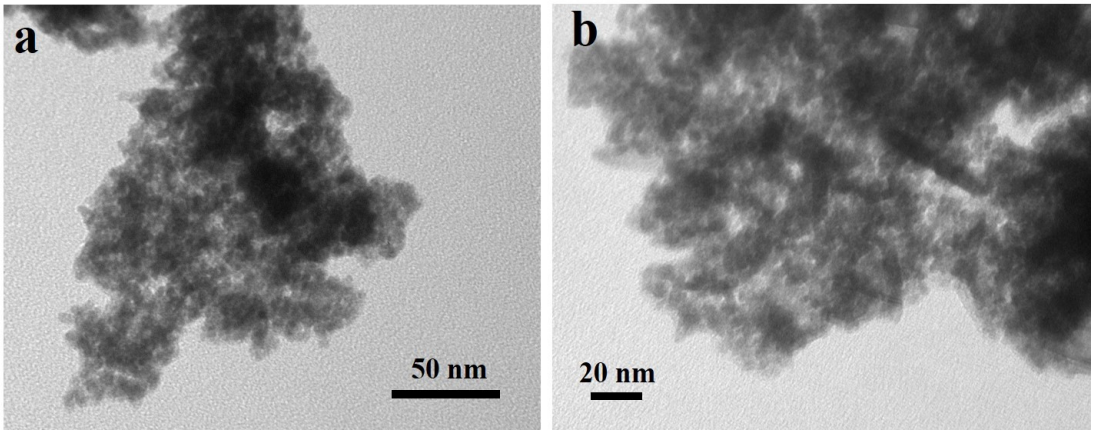

Figure S23. TEM images of the $In_{0.14}Ru_{0.86}O_2$-250 after OER.

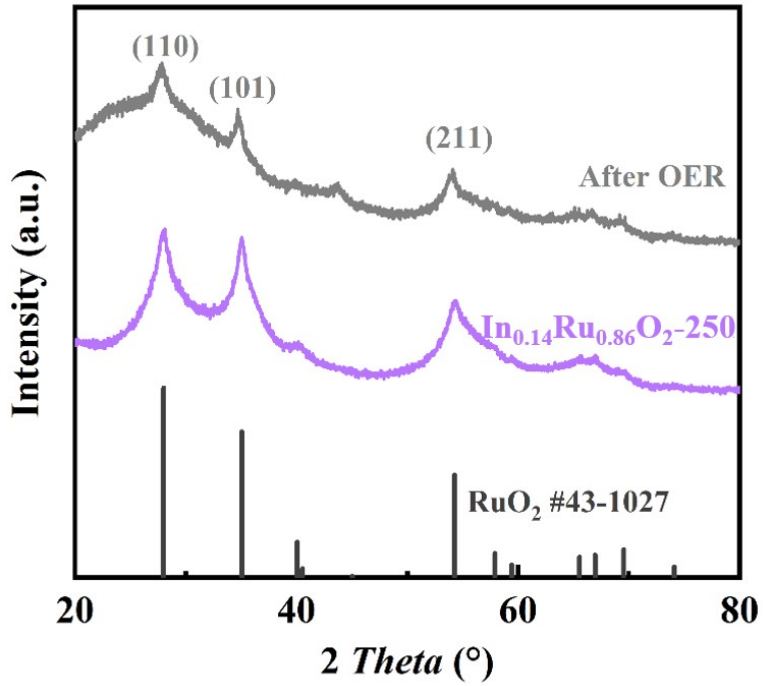

Figure S24. The XRD patterns of $In_{0.14}Ru_{0.86}O_2$-250 sample before and after OER.

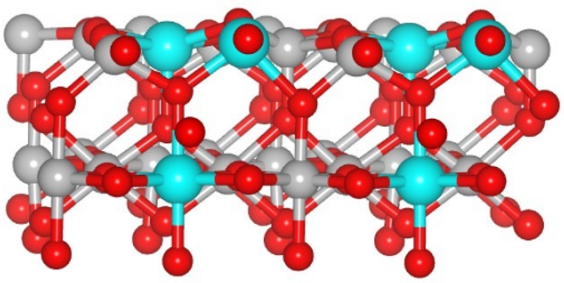

Figure S25. The model of the $In_3Ru_{13}O_{32}$, the gray, red and blue balls represent Ru, O and In atoms, respectively.

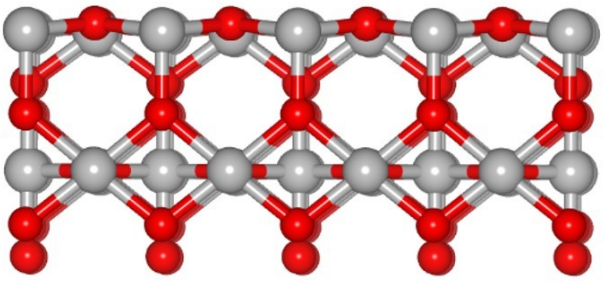

Figure S26. The model of the pure RuO_2, the gray and red balls represent Ru and O atoms, respectively.

Table S1. Peak assignments from deconvolution of high resolution Ru 3p XPS spectra of RuO_2-350 and $In_xRu_yO_2$-n samples.

	Ru $3p_{3/2}$ (eV)		**Ru $3p_{1/2}$ (eV)**	
	Ru^{4+}	**Ru^{n+}(n>4)**	**Ru^{4+}**	**Ru^{n+}(n>4)**
RuO_2-350	463.26	465.92	485.57	488.17
$In_{0.14}Ru_{0.86}O_2$-250	463.19	465.63	485.49	487.82
$In_{0.17}Ru_{0.83}O_2$-350	463.06	465.72	485.37	487.98
$In_{0.18}Ru_{0.82}O_2$-450	463.05	465.75	485.39	487.81

Table S2. Peak assignments from deconvolution of high resolution In 3d XPS spectra of In_2O_3 and $In_xRu_yO_2$-n samples.

	In $3d_{5/2}$ (eV)	**In $3d_{3/2}$ (eV)**
In_2O_3	444.49	452.09
$In_{0.14}Ru_{0.86}O_2$-250	444.94	452.54
$In_{0.17}Ru_{0.83}O_2$-350	445.01	452.61
$In_{0.18}Ru_{0.82}O_2$-450	444.95	452.55

Table S3. Peak assignments from deconvolution and corresponding content of high resolution O 1s XPS spectra of RuO_2-350 and $In_xRu_yO_2$-n samples.

	Lattice oxygen (eV)	**Oxygen defects (eV)**	**Adsorbed oxygen (eV)**
RuO_2-350	530.17	531.17	532.64
	36.4 %	33.8 %	29.8 %
$In_{0.17}Ru_{0.83}O_2$-350	530.12	531.18	532.37
	40.3 %	31.0 %	28.7 %

Table S4. Comparison of the electrocatalytic activities of RuO_2-350, $In_xRu_yO_2$-n samples and In_2O_3-RuO_2 Mixture for acid OER.

	Potential@10 mA cm^{-2} (mV)	**Potential@100 mA cm^{-2} (mV)**
RuO_2-350	184	358
$In_{0.14}Ru_{0.86}O_2$-250	180	323
$In_{0.17}Ru_{0.83}O_2$-350	177	298
$In_{0.18}Ru_{0.82}O_2$-450	206	341
In_2O_3-RuO_2 Mixture	334	——
In_2O_3	——	——

Table S5. Comparison of the Tafel slope of RuO_2-350, $In_xRu_yO_2$-n samples and In_2O_3-RuO_2 Mixture for acid OER.

	RuO_2-350	**$In_{0.14}Ru_{0.86}O_2$-250**	**$In_{0.17}Ru_{0.83}O_2$-350**	**$In_{0.18}Ru_{0.82}O_2$-450**	**In_2O_3-RuO_2 Mixture**
Tafel slope (mV/dec)	84.46	97.65	32.62	63.54	261.9

Table S6. Comparison of the C_{dl}, ECSA and RF of RuO_2-350, $In_xRu_yO_2$-n samples and In_2O_3-RuO_2 Mixture for acid OER.

	RuO_2-350	**$In_{0.14}Ru_{0.86}O_2$-250**	**$In_{0.17}Ru_{0.83}O_2$-350**	**$In_{0.18}Ru_{0.82}O_2$-450**	**In_2O_3-RuO_2 Mixture**
C_{dl} (mF/cm^2)	8.32	16.39	53.99	10.28	0.79
ECSA (cm^2)	16.88	33.25	109.52	20.85	1.60
RF	237.71	468.29	1542.57	293.71	22.57

Table S7. TOF and TON of various catalysts.

Catalyst	**$In_{0.14}Ru_{0.86}O_2$-250**	**$In_{0.17}Ru_{0.83}O_2$-350**	**$In_{0.18}Ru_{0.82}O_2$-450**
TOF (s^{-1})	0.21	0.23	0.15
TON (1)	11.92	13.02	8.79

References

1. J. Su, R. Ge, K. Jiang, Y. Dong, F. Hao, Z. Tian, G. Chen and L. Chen, *Adv Mater*, 2018, DOI: 10.1002/adma.201801351, e1801351.
2. Y. Lin, Z. Tian, L. Zhang, J. Ma, Z. Jiang, B. J. Deibert, R. Ge and L. Chen, *Nat Commun*, 2019, **10**, 162.
3. S. Chen, H. Huang, P. Jiang, K. Yang, J. Diao, S. Gong, S. Liu, M. Huang, H. Wang and Q. Chen, *ACS Catalysis*, 2019, **10**, 1152-1160.
4. F. Y. Gao, S. J. Hu, X. L. Zhang, Y. R. Zheng, H. J. Wang, Z. Z. Niu, P. P. Yang, R. C. Bao, T. Ma, Z. Dang, Y. Guan, X. S. Zheng, X. Zheng, J. F. Zhu, M. R. Gao and S. H. Yu, *Angew Chem Int Ed Engl*, 2020, **59**, 8706-8712.
5. G. Kresse and J. Hafner, *Phys Rev B Condens Matter*, 1993, **48**, 13115-13118.
6. J. P. Perdew, K. Burke and M. Ernzerhof, *Phys Rev Lett*, 1996, **77**, 3865-3868.
7. I. C. Man, H. Y. Su, F. Calle‐Vallejo, H. A. Hansen, J. I. Martínez, N. G. Inoglu, J. Kitchin, T. F. Jaramillo, J. K. Nørskov and J. Rossmeisl, *ChemCatChem*, 2011, **3**, 1159-1165.